Chemical Science

ROYAL SOCIETY OF CHEMISTRY

EDGE ARTICLE

View Article Online
View Journal | View Issue

Cite this: *Chem. Sci.*, 2021, **12**, 11722

All publication charges for this article have been paid for by the Royal Society of Chemistry

Turning waste into wealth: facile and green synthesis of carbon nanodots from pollutants and applications to bioimaging†

Weifeng Chen,‡[a] Jialu Shen,‡[a] Zuo Wang,‡[b] Xiang Liu, *[a] Yanyi Xu,[b] Haiyu Zhao *[b] and Didier Astruc *[c]

Received 25th May 2021
Accepted 1st August 2021

DOI: 10.1039/d1sc02837e

rsc.li/chemical-science

In an effort to turn waste into wealth, Reactive Red 2 (RR2), a common and refractory organic pollutant in industrial wastewater, has been employed for the first time as a precursor to synthesize carbon nanodots (CNDs) by a facile, green and low-cost route, without utilization of any strong acids or other oxidizers. The detailed characterizations have confirmed that the synthesized CNDs exhibit good water dispersibility, with a mean particle size of 2.43 nm and thickness of 1–3 layers. Importantly, the excellent fluorescence properties and much reduced biotoxicity of the CNDs confer its potential applications in further biological imaging, which has been successfully verified in both *in vitro* (cell culture) and *in vivo* (zebrafish) model systems. Thus, it is demonstrated that the synthesized CNDs exhibit nice biocompatibility and fluorescence properties for bioimaging. This work not only provides a novel economical and environmentally friendly approach in recycling a chemical pollutant, but also greatly promotes the potential application of CNDs in biological imaging.

1. Introduction

Carbon nanodots (CNDs) have gained tremendous research attention worldwide due to their preeminent water solubility, highly tunable band gaps, superior photo and chemical stability, low cytotoxicity, excellent biocompatibility, easy functionalization, brilliant catalytic properties and high photoluminescence (PL) intensity.[1] These nanomaterials that usually possess heavily functionalized graphene-like structures[2] have been extensively applied in many areas including biomedical optical imaging, catalysis, heterojunction solar cells, drug delivery, environmental monitoring, supercapacitors and biosensing.[3] The synthesis of CNDs has been typically classified into top-down and bottom-up strategies. The top-down strategies involve the synthesis of CNDs from graphite, graphene nanosheets, carbon nanotubes, candle soot, coal and graphite rods by physical or chemical cutting treatment;[4] on the other hand, the bottom-up strategies target the fabrication of CNDs from conventional organic molecules or biomass by plasma treatment, ultrasonic/microwave irradiation, hydrothermal treatment or thermal decomposition.[5] However, many of these methods are associated with some demerits, such as high cost, low yields, time-consuming processes, or the utilization of strong acids.[6] Therefore, it is still a considerable challenge to develop more facile and green approaches for the synthesis of CNDs from abundant and low-cost precursors.

The rapidly increasing usage of organic dyes (*e.g.*, reactive red 2) in industrial manufacture, such as textile, papermaking, plastics, pigments and paint, has rendered them among the most globally hazardous pollutants of water.[7] Approximately 10% of organic dyes containing aromatic groups and azo groups (–N=N–) have been discharged into natural water.[8] The mass discharge of these azo dyes represents a great threat for aquatic organisms and ecological environments since most of azo dyes are highly toxic, carcinogenic and teratogenetic.[9] A large number of methods, such as ozonation, biological treatment, ionic exchange, photocatalysis, oxidative process and adsorption have been developed for the removal of organic dyes from water.[10] However, these efforts are always associated with high chemical and energy consumption, as well as costly equipment investment. Therefore, developing more eco-friendly and efficient tactics for the removal of the organic dyes and turning these chemical pollutants into wealth is still a very meaningful and challenging research.[11]

[a]*College of Materials and Chemical Engineering, Engineering Research Center of Eco-environment in Three Gorges Reservoir Region, Ministry of Education, Key Laboratory of Inorganic Nonmetallic Crystalline and Energy Conversion Materials, China Three Gorges University, Yichang, Hubei 443002, P. R. China. E-mail: xiang.liu@ctgu.edu.cn*

[b]*Gansu Key Laboratory of Biomonitoring and Bioremediation for Environmental Pollution, School of Life Sciences, Lanzhou University, Lanzhou, Gansu, 730000, P. R. China. E-mail: zhaohy@lzu.edu.cn*

[c]*ISM, UMR CNRS No. 5255, Univ. Bordeaux, 351 Cours de la Libération, 33405 Talence Cedex, France. E-mail: didier.astruc@u-bordeaux.fr*

† Electronic supplementary information (ESI) available. See DOI: 10.1039/d1sc02837e

‡ These authors have equally contributed to this work and should be considered as co-first authors.

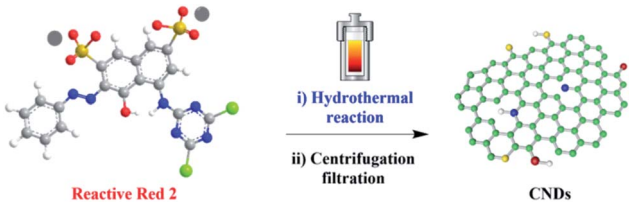

Fig. 1 The synthesis of CNDs from reactive red 2.

For this purpose, our laboratories have a long-term interest in the synthesis of carbon nanodots from abundant and low-cost biomass and their applications in catalysis, sensor and bioimaging.[12] Herein, we report a facile, green and turning wastes into wealth route to synthesize the typical material carbon nanodots (CNDs) by using chemical pollutant reactive red 2 (RR2) as the precursor for the first time, *via* simple hydrothermal treatment (Fig. 1). Thereafter, the morphology structure, fluorescence properties and chemical composition of the as-synthesized CNDs have been comprehensively investigated. Importantly, this work provides some insights into the biotoxicity of the synthesized CNDs in comparison with the RR2 precursor, at the cellular and organismal level. Our results verified that the biotoxicity was dramatically reduced when the pollutant was fully converted into CNDs. In addition, the synthesized CNDs with excellent fluorescent properties have been successfully applied in the bioimaging of both living cell and the popular zebrafish model system, demonstrating practically biological applications in the future.

2. Results and discussion

2.1 Structural characterization of the CNDs

First, the CNDs were synthesized from only RR2 and water under green hydrothermal conditions. Indeed, RR2 was successfully fully converted into CNDs, because the adsorption peak at approximately 500 nm and the characteristic peaks of RR2 completely disappeared in the UV-vis spectra (Fig. 2). Meanwhile, the peaks at 234 nm, 269 nm and 358 nm (the characteristic peaks of CNDs) appeared in the UV-vis spectra.

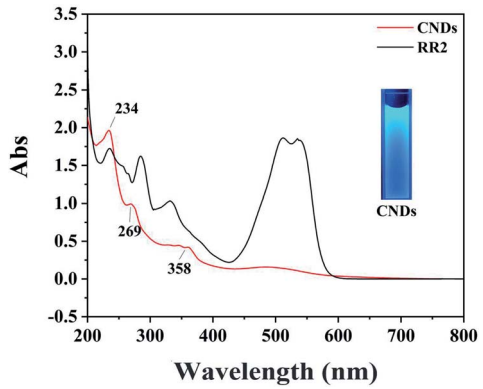

Fig. 2 UV-vis spectra of RR2 and CNDs; inset image: CNDs solution exhibits intense blue fluorescence under 365 nm ultraviolet lamp.

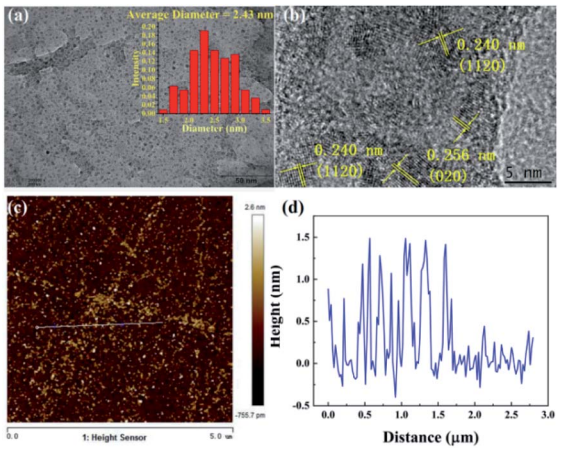

Fig. 3 (a) TEM image, (b) HRTEM image, (c) AFM image, and (d) height profile of CNDs.

Among them, the peaks at 234 nm and 269 nm are assigned to π–π* transitions of C=C/C–C bonds in the sp^2 hybridization region, while the peak of 358 nm is due to the n–π* transition.[13] The CNDs solution exhibited an intense blue fluorescence under 365 nm ultraviolet lamp (Fig. 2). The transmission electron microscope (TEM) image shows that the CNDs are well dispersed with an average diameter of 2.43 nm (Fig. 3a). Besides, the interplanar spacings of 0.240 nm and 0.256 nm were observed by high resolution TEM (HRTEM, Fig. 3b), and assigned to the (1120) and (020) plane of graphitic carbon, respectively (JCPDS 26-1076).[14] The atomic force microscope (AFM) image of CNDs (Fig. 3c) indicates that the height is less than 1.5 nm (Fig. 3d), suggesting that the thickness of CNDs is 1–3 layers.[15] Then, X-ray photoelectron spectroscopy (XPS) was utilized to study the valence states of the different atoms of CNDs, *i.e.*, C, N, O, and S (Fig. 4). The spectrum of C 1s (Fig. 4a) shows the typical peaks at 284.8 eV, 286.27 eV and 288.84 eV corresponding to C=C/C–C, C–O–C and O–C=O, respectively.[16]

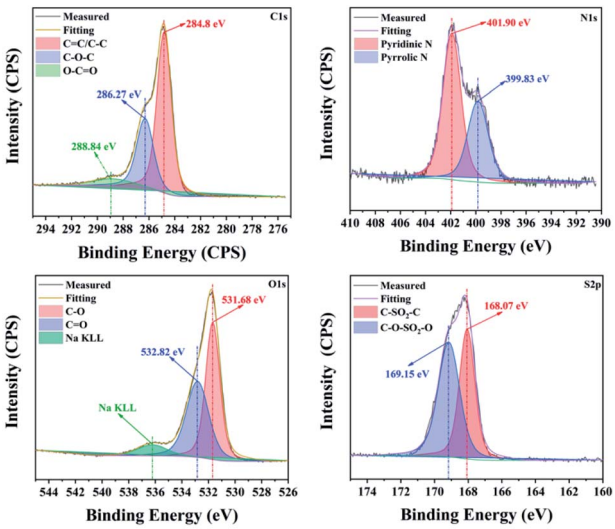

Fig. 4 The C 1s, N 1s, O 1s, and S 2p XPS of CNDs.

Moreover, the XPS of N 1s (Fig. 4b) exhibited two peaks at 399.83 eV and 401.90 eV belonging to the pyrrolic N and pyridinic N, respectively. As shown in Fig. 4c, two characteristic peaks at 531.68 eV and 532.82 eV are assigned to C–O and C=O, respectively. Besides, the XPS spectrum of S 2p (Fig. 4d) shows that the S 2p spectra is decomposed into two peaks, C–SO_2–C at 168.07 eV and C–O–SO_2–O at 169.15 eV, respectively.

The structure of the produced CNDs was further investigated by Raman spectroscopy (Fig. 5a), revealing that the peaks of the D-band, G-band and 2D-band of the CNDs are located at 1300 cm^{-1}, 1584 cm^{-1} and 2778 cm^{-1}, respectively. The D-band and 2D-band are due to the disordered carbon, while the G-band is assigned to the graphite carbon. The value of I_D/I_G is 1.7, indicating the CNDs have some defects in the crystal lattices.[17] Fourier transform infrared spectroscopy (FT-IR) was also been used to investigate the chemical groups of CNDs, as shown in Fig. 5b. The peak at 3418 cm^{-1} is corresponding to the stretching vibration of O–H/N–H, whereas the characteristic peaks of 3166 cm^{-1}, 1660 cm^{-1}, 1405 cm^{-1}, 1055 cm^{-1} and 1624 cm^{-1} are attributed to the stretching vibrations of C–H, C=O, C–N and C–O, and bending vibration of N–H, respectively. Fig. 5c also exhibits a typical profile with a broad peak at approximately 24°, the characteristic peak of (002) graphene appears in the X-ray diffraction (XRD) spectrum (JCPDS card no. 75-0444). In addition, it indicates that the synthesized CNDs solution shows excitation-dependent PL property, as shown in Fig. 5d. When the excitation wavelength is set from 300 nm to 580 nm, the emission wavelength is improved from 423 nm to 619 nm. The maximum emission is at the position of 428 nm when being excited by 360 nm. In this work, rhodamine B in ethanol (QY = 69.0%) was used as a standard for CNDs. The quantum yield (QY) of CNDs was calculated to be 15.7%.[18] The fluorescence of CNDs is mainly attributed to emission from oxygen-rich surface defects.[19] To sum up, these results confirmed that the graphene-like structure containing sp^2 hybridization of these fluorescent CNDs has been formed from RR2 by hydrothermal reaction.

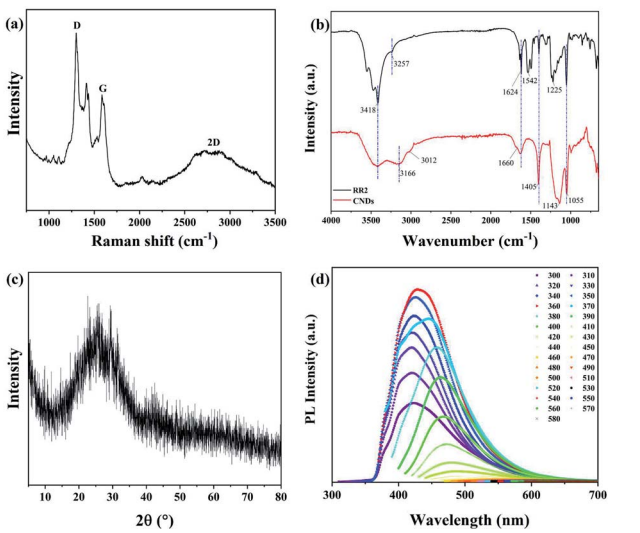

Fig. 5 (a) Raman spectrum, (b) FT-IR spectra, (c) XRD and (d) corresponding PL spectra at different excitation wavelengths from 300 nm to 580 nm for CNDs.

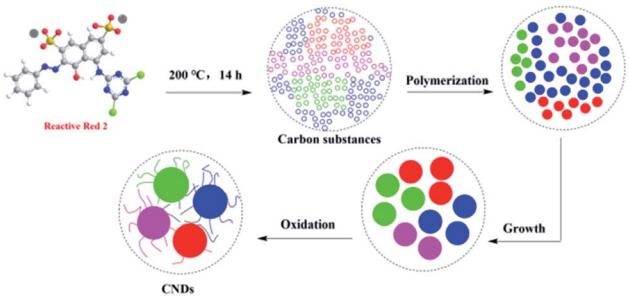

Fig. 6 Proposed mechanism of CNDs formation from RR2.

The formation mechanism of CNDs from RR2 involves two steps (Fig. 6); first RR2 was decomposed into small carbon substances under hydrothermal conditions. Then the small carbon substances were polymerized, grown and oxidized into these fluorescent CNDs with abundant surface O, N and S-containing functional groups. Finally, the fluorescence of CNDs is mainly attributed to these highly functional surface groups.[19,20]

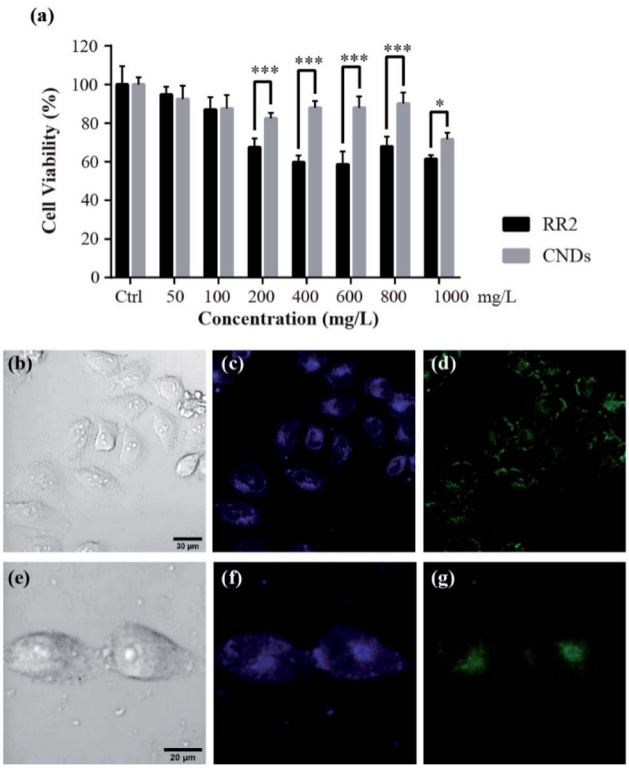

Fig. 7 Cytotoxicity assessment and fluorescence imaging. (a) Effect of the same amount of RR2 and CNDs on HeLa cell viability. MTT cell viability assay was performed in HeLa cells after RR2 and CNDs exposure (0–1000 mg L^{-1}) for 24 hours. Concentrations are plotted on the *X* axes, cell viability (%) ± SEM ($n = 6$) with respect to untreated cells (Ctrl) is plotted on the *Y* axes. Significant differences are indicated by asterisks (***$p < 0.001$, **$p < 0.01$, *$p < 0.05$). (b–g) Confocal fluorescence images of Hela cells (bright field images, b and e) stained with CNDs (100 mg L^{-1}, 24 hours) at the excitation of 405 (c and f) and 488 nm (d and g) laser beams respectively.

2.2 Cell viability

To test whether the cytotoxicity of the synthesized CNDs has been significantly reduced in comparison with the RR2, as well as its suitability for biological applications, we evaluated their cytotoxicity on HeLa cells by using a MTT assay. The HeLa cells were treated with RR2 and CNDs respectively for 24 h, and the MTT assay was performed to analyze their effect on cell viability. In comparison with the control (Ctrl) group, RR2 induced decreases in the viability of the HeLa cells in a dose-dependent manner, it reduced the cell viability by nearly 60% at the concentration of 1000 mg L^{-1}. However, the CNDs showed significantly reduced cytotoxicity ($p < 0.05$ or $p < 0.001$). It was so especially at high doses (above 200 mg L^{-1}), the average cell viability being greater than 70% even when they were treated with CNDs at a concentration of up to 1000 mg L^{-1} (Fig. 7a). This reveals the great bio-compatibility of the synthesized CNDs.

2.3 Living cells fluorescence imaging

Living cell fluorescence imaging was performed to demonstrate their practicability in biological applications.[21] The zeta potential value of CNDs is −24.1 mV (Fig. S2†), suggesting that the as-synthesized CNDs are relatively stable.[22] After incubating the HeLa cells with CNDs (100 mg L^{-1}) for 24 h at 37 °C, a significant fluorescence in the HeLa cells was observed (Fig. 7b–i). The CNDs were mostly localized at the cytoplasm of HeLa cells, since the cytoplasmic area exhibited a strong photoluminescence. Importantly, no photobleaching was observed within one hour for the cell imaging, suggesting that they are suitable for long-term cellular imaging. In addition, distinctive colors were available for the observation of the cells incubated with CNDs when they were excited with 405 nm and 488 nm laser beams, respectively. This intrinsic excitation separation property is particularly ideal for multichannel imaging, suggesting that CNDs are an excellent counterstain in cooperation

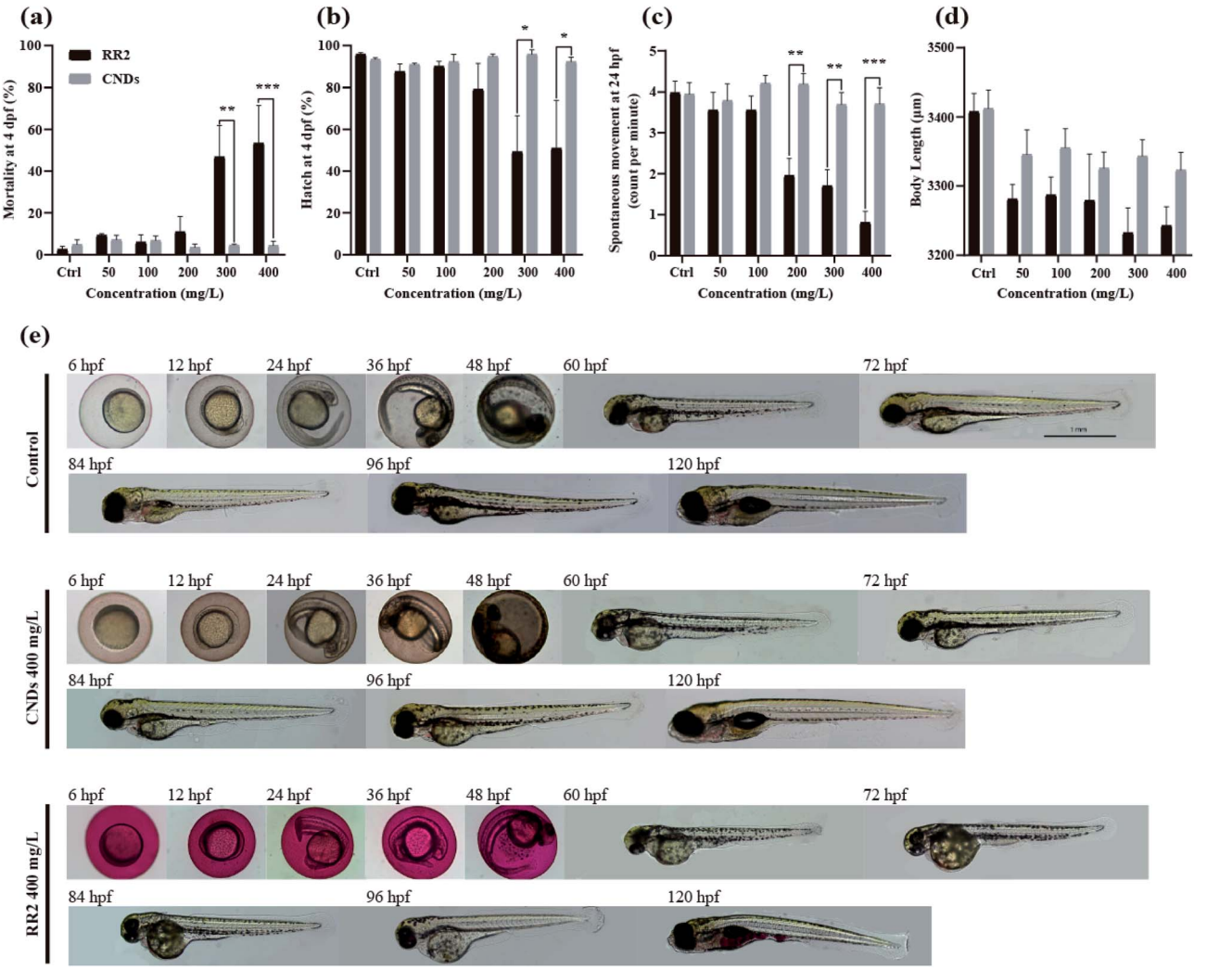

Fig. 8 Developmental toxicity of RR2 and CNDs to zebrafish embryos. Mortality rates (a), hatching rates (b), spontaneous movement (c) and body length (d) of zebrafish embryos exposed to increasing concentrations of RR2 and CNDs (*$p < 0.05$, **$p < 0.01$, ***$p < 0.001$). (e) Representative optical morphological images of zebrafish embryos exposed to RR2 and CNDs (400 mg L^{-1}) up to 120 hpf. No significant difference was observed between control and CNDs group, whereas significant reduction of body length and obvious yolk sac edema was shown in the RR2 treatment group.

with other dyes to obtain cellular images. This robust photostability as well as the multichannel tunability of our synthesized CNDs will certainly be beneficial for bioimaging applications.

2.4 Biotoxicity assay with the zebrafish model

The wide range applications of carbon nanodots in biomedical studies have attracted significant attention of the potential hazards to biological systems.[23] Zebrafish has been widely reported as a valuable vertebrate model and "gold standard" for assessing genotoxicity and developmental toxicity of chemicals and pollutants due to its high fecundity, cost-effectiveness, well-characterized developmental stages, and optical transparency.[24] Therefore, in this study the biotoxicity of RR2 and CNDs was systematically examined by exposing zebrafish embryos at 4 hpf to different concentrations of each regents for at least 120 hours. As shown in Fig. 8a, RR2 significantly induced mortality of zebrafish embryos at higher doses (above 300 mg L^{-1}). The hatching rate (at 4 dpf, Fig. 8b), spontaneous movement (at 24 hpf, Fig. 8c) and body length (at 4 dpf, Fig. 8d) of zebrafish embryos also declined significantly after exposure to RR2, in a dose dependent manner. However, within 120 hours, zebrafish embryos exposed to the CNDs (from 50 to 400 mg L^{-1}) were observed to develop normally without any sign of lethality and delay of hatching, no significant difference was observed between the CNDs treatment group and control group (Fig. 8a–d, grey panels). In addition, there were no noticeable influence on the morphology of zebrafish after exposure to different concentrations of CNDs, in sharp contrast with the RR2 treatment group, in which the body length of zebrafish was significantly reduced, and the yolk sac edema was obvious (Fig. 8e). All these notable morphological differences implied that in comparison with the RR2, the biotoxicity of CNDs was significantly reduced, and the CNDs (up to 400 mg L^{-1}) had no potential toxicity hazard to zebrafish development. CNDs have been reported to be unable to infiltrate the cell nucleus, which suggested that they did not disrupt the genetic structure of the organisms and caused cellular toxicity. This supports the hypotoxicity of our CNDs and its bio-compatibility for further utilization.

2.5 Neurobehavioral alteration induced by RR2 and CNDs

To further evaluate the developmental toxicity of RR2 and our synthesized CNDs, the neurobehavior of the zebrafish larvae exposed chronically was tested.[25] Specifically, we detected their locomotor activity as well as the response to environmental signals, for example light and vibration stimulations. The swimming speed, distance moved, cumulative mobility as well as maximum acceleration of zebrafish larvae was quantified in different assays. In our results, the developmental exposure to RR2 (200 mg L^{-1}) caused behavioral impairment including hypoactivity in locomotor activity as well as reduced reactivity to light–dark cycles. The swimming behaviors was significantly repressed by RR2 exposure especially during the dark period (Fig. 9a–d, black and blue traces, $p < 0.05$). Similarly, in the experiment testing the zebrafish response to vibration stimulations, a significant hypoactivity in swimming activity was observed in the RR2 exposure group during the whole process (Fig. 8e–h, black and blue traces, $p < 0.05$). However, in contrast to the RR2 that dramatically decreased the activity as well as the

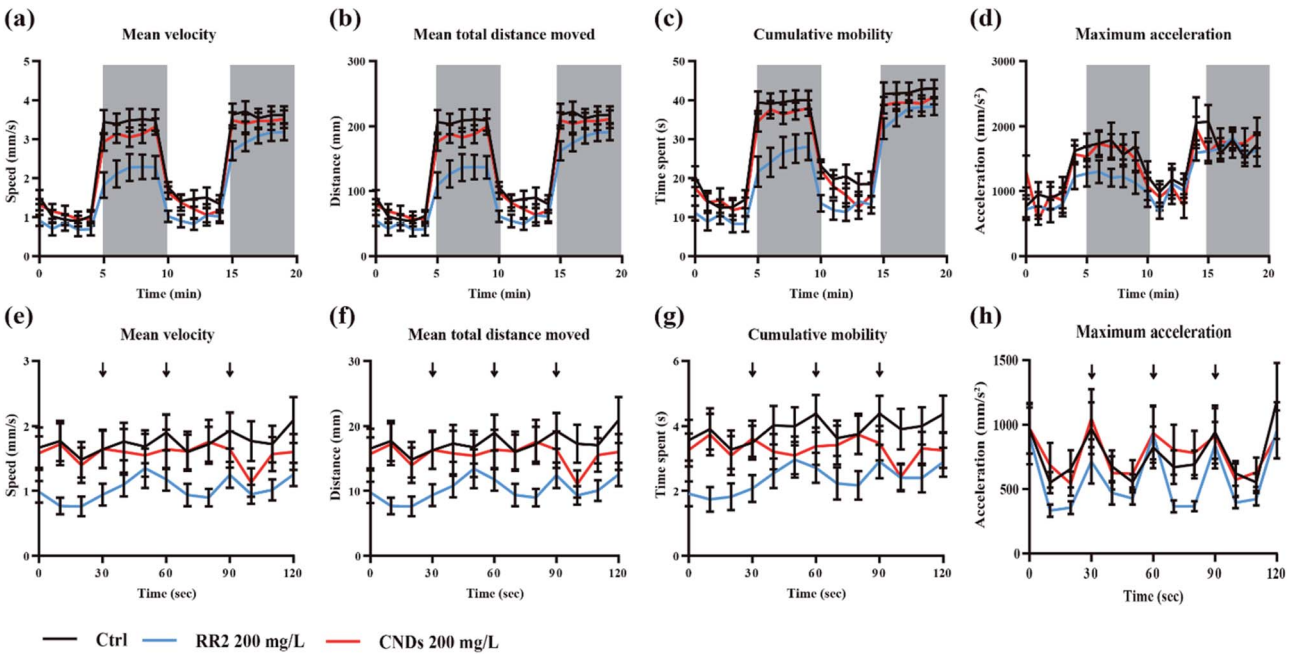

Fig. 9 Behavioral patterns of the zebrafish larvae from the control group (black traces), RR2 and (200 mg L^{-1}, blue traces) CNDs exposure (200 mg L^{-1}, red traces) groups during the light–dark photoperiod stimulation test (a–d) and typing stimulation (e–h) test. Data are expressed as mean ± SEM ($n = 24$). The white and gray shadows indicate the light and dark period respectively. The arrows indicate the time when typing vibration is induced.

Table 1 The developmental toxicity studies of zebrafish after exposure to different concentrations of RR2 and CNDs

Toxicological criteria	Timepoints	Exposure concentrations (mg L^{-1})	Results
Survival rates (mortality)	4 hpf to 5 dpf	0, 50, 100, 200, 300, 400	Fig. 8a
Hatching rates	2 dpf to 5 dpf	0, 50, 100, 200, 300, 400	Fig. 8b
Spontaneous movement	24 hpf	0, 50, 100, 200, 300, 400	Fig. 8c
Body length	96 hpf	0, 50, 100, 200, 300, 400	Fig. 8d
Morphological feature	6 hpf to 120 hpf	400	Fig. 8e
Behavioral test	24 hpf, 6 dpf	0, 50, 100, 200, 300, 400	Fig. 9

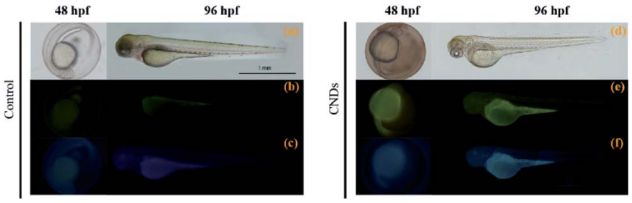

Fig. 10 Fluorescent imagings of zebrafish embryos (48 hpf) and larvae (96 hpf) after exposure to CNDs solution (400 mg L^{-1}, right panel), in comparison with control group (autofluorescence signal, left panel). (a and d) Bright field; (b and e) green fluorescent field; (c and f) blue fluorescent field.

reactivity, no significant difference was observed between the Ctrl group and the CNDs exposure group (Fig. 9a–h, black and red traces, $p > 0.05$). These results are consistent with the previous morphological observations showing the hypotoxicity of these synthesized CNDs, suggesting that they significantly elevated bio-compatibility (Table 1).

2.6 Fluorescence imaging of CNDs in zebrafish model

The rapid development and transparency of zebrafish embryos facilitate the application of CNDs in the biological imaging.[26] The imaging was implemented by acute exposing zebrafish embryos in CNDs solution (400 mg L^{-1}). Multicolor fluorescence imaging of zebrafish at different developmental stages (48 hpf and 96 hpf) was shown in Fig. 10. The small size of CNDs (2.4 nm), much smaller than the nanoscale pores of the zebrafish chorion (approximately 0.17 μm^2), enables their rapid entrance into the pores of the chorion upon simple immersion. In addition, the zebrafish embryo or larvae exhibited green and blue fluorescence under different excitation fields, and the multicolor fluorescent CNDs enabled the *in vivo* observation of their distribution in zebrafish embryos and larvae. This phenomenon indicates that the CNDs present high biocompatibility during zebrafish development and might be used as an excellent candidate for *in vivo* fluorescence imaging in biological studies.

3. Conclusions

In summary, a facile, green and low-cost synthesis of carbon nanodots from the chemical pollutant reactive red 2 has allowed various full-scale biological assays demonstrating that the biotoxicity of the CNDs was significantly reduced in the cellular as well as organismal levels in comparison to its azo dye precursor, in which azo groups are the main cause of cytotoxicity.[27] The fluorescence properties and low cytotoxicity of the synthesized CNDs confer its very favorable potential applications in biological imaging, as verified in the *in vitro* (cell culture) and *in vivo* (zebrafish embryo) model systems. In an effort to turn waste into wealth, the discovery of CNDs from RR2 provides new economically and environmentally friendly opportunities in both bioimaging and waste-water remediation.

Ethical statement

All zebrafish husbandry and experimental procedures were performed in accordance with the Guiding Principles for the Care and Use of Laboratory Animals and were reviewed and approved by the Animal Care Committee of Lanzhou University (ethic approval ID no. EAF2020007).

Data availability

All data, models, or code generated or used during the study are available from the corresponding author by request.

Author contributions

X. L., D. A. and H. Z. conceived this project; W. C., J. S., Z. W. and Y. X. performed the experiments; X. L., D. A. and H. Z. analyzed the data and wrote the paper. All authors provided scientific input, edited, and approved the final manuscript.

Conflicts of interest

There are no conflicts to declare.

Acknowledgements

Funding by the National Natural Science Foundation of China (21805166), the 111 Project (D20015) and the Engineering Research Center of Eco-environment in Three Gorges Reservoir Region, Ministry of Education, China Three Gorges University (KF2019-05), the outstanding young and middle-aged science and technology innovation teams, Ministry of Education, Hubei province, China (T2020004), Foundation of Science and Technology Bureau of Yichang City (A21-3-012), the Fundamental Research Funds for the Central Universities (lzujbky-2019-74), the "Double First-Class" Research Start-up Funds of Lanzhou University (561119203), the University of Bordeaux and the

Centre National de la Recherche Scientifique (CNRS) is gratefully acknowledged.

Notes and references

1 (*a*) M. J. H. Ku, T. X. Zhou, Q. Li, Y. J. Shin, J. K. Shi, C. Burch, L. E. Anderson, A. T. Pierce, Y. Xie, A. Hamo, U. Vool, H. Zhang, F. Casola, T. Taniguchi, K. Watanabe, M. M. Fogler, P. Kim, A. Yacoby and R. L. Walsworth, *Nature*, 2020, **583**, 537–541; (*b*) A. El Fatimy, R. L. Myers-Ward, A. K. Boyd, K. M. Daniels, D. K. Gaskill and P. Barbara, *Nat. Nanotechnol.*, 2016, **11**, 335–338; (*c*) M. Kaur, M. Kaur and V. K. Sharma, *Adv. Colloid Interface Sci.*, 2018, **259**, 44–64; (*d*) J. Zhu, Y. Tang, G. Wang, J. Mao, Z. Liu, T. Sun, M. Wang, D. Chen, Y. Yang, J. Li, Y. Deng and S. Yang, *ACS Appl. Mater. Interfaces*, 2017, **9**, 14470–14477.

2 (*a*) A. Cadranel, J. T. Margraf, V. Strauss, T. Clark and D. M. Guldi, *Acc. Chem. Res.*, 2019, **52**, 955–963; (*b*) X. Xu, R. Ray, Y. Gu, H. J. Ploehn, L. Gearheart, K. Raker and W. A. Scrivens, *J. Am. Chem. Soc.*, 2018, **126**, 12736–12737; (*c*) X. Xu, R. Ray, Y. Gu, H. J. Ploehn, L. Gearheart, K. Raker and W. A. Scrivens, *J. Am. Chem. Soc.*, 2004, **126**, 12736–12737; (*d*) Y.-P. Sun, B. Zhou, Y. Lin, W. Wang, K. A. Fernando, P. Pathak, M. J. Meziani, B. A. Harruff, X. Wang, H. Wang, P. G. Luo, H. Yang, M. E. Kose, B. Chen, L. M. Veca and S. F. Xie, *J. Am. Chem. Soc.*, 2006, **128**, 7756–7757; (*e*) M. Zhang, X. Zhai, M. Sun, T. Ma, Y. Huang, B. Huang, Y. Du and C. Yan, *Chem. Soc. Rev.*, 2020, **49**, 9220–9248; (*f*) F. Arcudi, L. Đorđević and M. Prato, *Acc. Chem. Res.*, 2019, **52**, 2070–2079; (*g*) V. S. Sivasankarapillai, A. V. Kirthi, M. Akksadha, S. Indu, U. D. Dharshini, J. Pushpamalar and L. Karthik, *Nanoscale Adv.*, 2020, **2**, 1760–1773; (*h*) Z. Hassanvand, F. Jalali, M. Nazari, F. Parnianchi and C. Santoro, *ChemElectroChem*, 2021, **8**, 15–35; (*i*) C. Liu, F. Zhang, J. Hu, W. Gao and M. Zhang, *Front. Chem.*, 2021, **8**, 605028.

3 (*a*) Y.-T. Long and T. J. Meade, *Chem. Sci.*, 2020, **11**, 6940–6941; (*b*) J. Wang, X. Wu, J. Pan, T. Feng, D. Wu, X. Zhang, B. Yang, X. Zhang and J. Jie, *Adv. Mater.*, 2020, **32**, 2003315; (*c*) Y. Uemura, K. Yamato, R. Sekiya and T. Haino, *Angew. Chem., Int. Ed.*, 2018, **57**, 4960–4964; (*d*) W. Xu, D. Wang and B. Z. Tang, *Angew. Chem., Int. Ed.*, 2021, **60**, 7476–7487; (*e*) J. H. Zhang, T. Sun, A. Niu, Y. M. Tang, S. Deng, W. Luo, Q. Xu, D. Wei and D. S. Pei, *Biomaterials*, 2017, **133**, 49–59; (*f*) S. Deng, P. P. Jia, J. H. Zhang, M. Junaid, A. Niu, Y. B. Ma, A. Fu and D. S. Pei, *J. Hazard. Mater.*, 2018, **357**, 146–158.

4 (*a*) Y. Yan, J. Gong, J. Chen, Z. Zeng, W. Huang, K. Pu, J. Liu and P. Chen, *Adv. Mater.*, 2019, **31**, 1808283; (*b*) G. Gollavelli and Y. C. Ling, *Biomaterials*, 2012, **33**, 2532–2545.

5 (*a*) S. Deng, A. Fu, M. Junaid, Y. Wang, Q. Yin, C. Fu, L. Liu, D. S. Su, W. P. Bian and D. S. Pei, *Biomaterials*, 2019, **206**, 61–72; (*b*) Y. F. Huang, X. Zhou, R. Zhou, H. Zhang, K. B. Kang, M. Zhao, Y. Peng, Q. Wang, H. L. Zhang and W. Y. Qiu, *Chem.–Eur. J.*, 2014, **20**, 5640–5648; (*c*) X. Wei, L. Li, J. Liu, L. Yu, H. Li, F. Cheng, X. Yi, J. He and B. Li, *ACS Appl. Mater. Interfaces.*, 2019, **11**, 9832–9840; (*d*) S. Li, Z. Peng, J. Dallman, J. Baker, A. M. Othman, P. L. Blackwelder and R. M. Leblanc, *Colloids Surf., B*, 2016, **145**, 251–256; (*e*) S. Li, I. Skromne, Z. Peng, J. Dallman, A. O. Al-Youbi, A. S. Bashammakh, M. S. El-Shahawi and R. M. Leblanc, *J. Mater. Chem. B*, 2016, **4**, 7398–7405; (*f*) F. Huo, W. Liang, Y. Tang, W. Zhang, X. Liu, D. Pei, H. Wang, W. Jia, P. Jia and F. Yang, *J. Mater. Sci.*, 2019, **54**, 6815–6825; (*g*) S. Y. Park, C. Y. Lee, H. R. An, H. Kim, Y. C. Lee, E. C. Park, H. S. Chun, H. Y. Yang, S. H. Choi, H. S. Kim, K. S. Kang, H. G. Park, J. P. Kim, Y. Choi, J. Lee and H. U. Lee, *Nanoscale*, 2017, **9**, 9210–9217; (*h*) Z. Zhu, J. Qian, X. Zhao, W. Qin, R. Hu, H. Zhang, D. Li, Z. Xu, B. Z. Tang and S. He, *ACS Nano*, 2016, **10**, 588–597.

6 (*a*) C.-L. Huang, C.-C. Huang, F.-D. Mai, C.-L. Yen, S.-H. Tzing, H.-T. Hsieh, Y.-C. Ling and J.-Y. Chang, *J. Mater. Chem. B*, 2015, **3**, 651–664; (*b*) P. Roy, A. P. Periasamy, C. Y. Lin, G. M. Her, W. J. Chiu, C. L. Li, C. L. Shu, C. C. Huang, C. T. Liang and H. T. Chang, *Nanoscale*, 2017, **7**, 2504–2510; (*c*) L. Ma, Y. Gao and X. Hu, *Biomaterials*, 2015, **52**, 301–311; (*d*) S. H. Chiu, G. Gedda, W. M. Girma, J. K. Chen, Y. C. Ling, A. V. Ghule, K. L. Ou and J. Y. Chang, *Acta Biomater.*, 2016, **46**, 151–164; (*e*) F. Du, Z. Cheng, M. Kremer, Y. Liu, X. Wang, S. Shuang and C. Dong, *J. Mater. Chem. B*, 2020, **8**, 5089–5095.

7 (*a*) F. Lu and D. Astruc, *Coord. Chem. Rev.*, 2018, **356**, 147–164; (*b*) F. Lu and D. Astruc, *Coord. Chem. Rev.*, 2020, **408**, 213180.

8 M. de la Luz-Asunción, E. E. Pérez-Ramírez, A. L. Martínez-Hernández, P. E. García-Casillas, J. G. Luna-Bárcenas and C. Velasco-Santos, *Diamond Relat. Mater.*, 2020, **109**, 108002.

9 (*a*) Z. Oruç, M. Ergüt, D. Uzunoğlu and A. Özer, *J. Environ. Chem. Eng.*, 2019, **7**, 103231; (*b*) Z. Wang, Q. Yin, M. Gu, K. He and G. Wu, *J. Hazard. Mater.*, 2018, **357**, 226–234.

10 (*a*) X. Liu, Y. Huang, P. Zhao, X. Meng and D. Astruc, *ChemCatChem*, 2020, **12**, 175–180; (*b*) Y. Huang, K. Zheng, X. Liu, X. Meng and D. Astruc, *Inorg. Chem. Front.*, 2020, **7**, 939–945; (*c*) J. Ma, X. Yang, X. Jiang, J. Wen, J. Li, Y. Zhong, L. Chi and Y. Wang, *Chem. Eng. J.*, 2020, **389**, 123422; (*d*) S. Ye, G. Zeng, X. Tan, H. Wu, J. Liang, B. Song, N. Tang, P. Zhang, Y. Yang, Q. Chen and X. Li, *Appl. Catal., B*, 2020, **269**, 118850; (*e*) L. Peng, Y. Shang, B. Gao and X. Xu, *Appl. Catal., B*, 2021, **282**, 119484; (*f*) S. Zhang, B. Li, X. Wang, G. Zhao, B. Hu, Z. Lu, T. Wen, J. Chen and X. Wnag, *Chem. Eng. J.*, 2020, **390**, 124642; (*g*) A. Tkaczyk, K. Mitrowska and A. Posyniak, *Sci. Total Environ.*, 2020, **717**, 37222; (*h*) W. Hou, S. Wang, X. Bi, X. Meng, P. Zhao and X. Liu, *Chin. Chem. Lett.*, 2021, DOI: 10.1016/j.cclet.2021.01.023; (*i*) L. Zhang, X. Bi, M. Gou, M. Sun, L. Tao, G. Chen, X. Liu, X. Meng and P. Zhao, *Sep. Purif. Technol.*, 2021, **264**, 118397; (*j*) X. Bi, Y. Huang, X. Liu, N. Yao, P. Zhao, X. Meng and D. Astruc, *Sep. Purif. Technol.*, 2021, **275**, 119141; (*k*) L. Peng, X. Duan, Y. Shang, B. Gao and X. Xu, *Appl. Catal., B*, 2021, **287**, 118863; (*l*) Y. Shang, X. Xu, B. Gao, S. Wang and X. Duan, *Chem. Soc. Rev.*, 2021, **50**, 5281–5322.

11 (*a*) J. Hu, X. Yuan, C. Wng, X. Shao, B. Yang, A. A. Razzaq, X. Zhao, Y. Lian, Z. Zhao, M. Chen and Y. Peng, *Small*, 2020, **16**, 2000755; (*b*) H. Xu, Y. Liu, Q. Bai and R. Wu, *J. Mater. Chem. A*, 2019, **7**, 3558–3562; (*c*) G. Ding, Y. Li, Y. Zhang, C. Huang, X. Yao, K. Lin, K. Shen, W. Yan, F. Sun and L. Zhou, *ACS Appl. Mater. Interfaces*, 2019, **11**, 19096–19103; (*d*) Y. Yao and F. Wu, *ACS Appl. Mater. Interfaces*, 2017, **9**, 31907–31912; (*e*) W. Yuan, A. Jie, S. Li, F. Huang, P. Zhang and Y. Shen, *Energy*, 2016, **115**, 397–403; (*f*) T. K. Marella, I. Y. López-Pacheco, R. Parra-Saldívar, S. Dixit and A. Tiwari, *Sci. Total Environ.*, 2020, **724**, 137960.

12 (*a*) W. Chen, D. Li, L. Tian, W. Xiang, T. Wang, W. Hu, Y. Hu, S. Chen, J. Chen and Z. Dai, *Green Chem.*, 2018, **20**, 4438–4442; (*b*) W. Chen, J. Shen, Y. Huang, X. Liu and D. Astruc, *ACS Sustainable Chem. Eng.*, 2020, **8**, 7513–7522; (*c*) J. Shen, W. Chen, G. Lv, Z. Yang, J. Yan, X. Liu and Z. Dai, *Int. J. Hydrogen Energy*, 2021, **46**, 796–805; (*d*) W. Chen, G. Lv, Q. Zhou, J. Shen, J. Cao, X. Liu and Z. Dai, *Nano Res.*, 2021, **14**, 1228–1231.

13 (*a*) C.-L. Shen, Q. Lou, J.-H. Zang, K.-K. Liu, S.-N. Qu, L. Dong and C.-X. Shan, *Adv. Sci.*, 2020, **7**, 1903525; (*b*) P. Roy, P.-C. Chen, A. P. Periasamy, Y.-N. Chen and H.-T. Chang, *Mater. Today*, 2015, **18**, 447–458.

14 (*a*) B. Kong, J. Tang, Y. Zhang, T. Jiang, X. Gong, C. Peng, J. Wei, J. Yang, Y. Wang, X. Wang, G. Zheng, C. Selomulya and D. Zhao, *Nat. Chem.*, 2016, **8**, 171–178; (*b*) C. Kgtahya, Y. Zhai, S. Li, S. Liu, J. Li, V. Strehmel, Z. Chen and B. Strehmel, *Angew. Chem., Int. Ed.*, 2021, **60**, 10983–10991; (*c*) N. Soni, S. Singh, S. Sharma, G. Batra, K. Kaushik, C. Rao, N. C. Verma, B. Mondal, A. Yadav and C. K. Nandi, *Chem. Sci.*, 2021, **12**, 3615–3626.

15 J. Liu, M. Zheng, X. Shi, H. Zeng and H. Xia, *Adv. Funct. Mater.*, 2016, **26**, 919–930.

16 S. Zhang, J. Zhu, Y. Qing, L. Wang, J. Zhao, J. Li, W. Tian, D. Jia and Z. Fan, *Adv. Funct. Mater.*, 2018, **28**, 1805898.

17 (*a*) Y.-C. Liang, K.-K. Liu, X.-Y. Wu, Q. Lou, L.-Z. Sui, L. Dong, K.-J. Yuan and C.-X. Shan, *Adv. Sci.*, 2021, **8**, 2003433; (*b*) Y. Gao, W. Xu, F. He, P. Nie, Q. Yang, Z. Si, H. Meng and G. Wei, *Nano Res.*, 2021, **14**, 2294–2300; (*c*) S.-Y. Song, L.-Z. Sui, K.-K. Liu, Q. Cao, W.-B. Zhao, Y.-C. Liang, C.-F. Lv, J.-H. Zang, Y. Shang, Q. Lou, X.-G. Yang, L. Dong, K. J. Yuan and C.-X. Shan, *Nano Res.*, 2021, **14**, 2231–2240; (*d*) S. Zhao, D. Zhang, S. Jiang, Y. Cui, H. Li, J. Dong, Z. Xie, D.-W. Wang, R. Amal, Z. Xia and L. Dai, *Nano Res.*, 2021, DOI: 10.1007/s12274-021-3358-3.

18 S. J. Zhu, Q. N. Meng, L. Wang, J. H. Zhang, Y. B. Song, H. Jin, K. Zhang, H. C. Sun, H. Y. Wang and B. Yang, *Angew. Chem., Int. Ed.*, 2013, **52**, 3953–3957.

19 (*a*) H. A. Nguyen, I. Srivastava, D. Pan and M. Gruebele, *ACS Nano*, 2020, **14**, 6127–6137; (*b*) N. C. Verma, A. Yadav, C. Rao, P. M. Mishra and C. K. Nandi, *J. Phys. Chem. C*, 2021, **125**, 1637–1653.

20 (*a*) S. Zhu, Y. Song, X. Zhao, J. Shao, J. Zhang and B. Yang, *Nano Res.*, 2015, **8**, 355–381; (*b*) B.-P. Qi, L. Bao, Z.-L. Zhang and D.-W. Pang, *ACS Appl. Mater. Interfaces*, 2016, **8**, 28372–28382; (*c*) H. Li, H. Ming, Y. Liu, H. Yu, X. He, H. Huang, K. Pan, Z. Kang and S.-T. Lee, *New J. Chem.*, 2011, **35**, 2666–2670; (*d*) L. Ai, Y. Yang, B. Wang, J. Chang, Z. Tang, B. Yang and S. Lu, *Sci. Bull.*, 2021, **66**, 839–856.

21 (*a*) S. N. Baker and G. A. Baker, *Angew. Chem., Int. Ed.*, 2010, **49**, 6726–6744; (*b*) P. G. Luo, S. Sahu, S.-T. Yang, S. K. Sonkar, J. Wang, H. Wang, G. E. LeCroy, L. Cao and Y.-P. Sun, *J. Mater. Chem. B*, 2013, **1**, 2116–2127; (*c*) K. Hola, Y. Zhang, Y. Wang, E. P. Giannelis, R. Zboril and A. L. Rogach, *Nano Today*, 2014, **9**, 590–603; (*d*) S. Zhu, J. Zhang, S. Tang, C. Qiao, L. Wang, H. Wang, X. Liu, B. Li, Y. Li, W. Yu, X. Wang, H. Sun and B. Yang, *Adv. Funct. Mater.*, 2012, **22**, 4732–4740; (*e*) S. Zhu, J. Zhang, C. Qiao, S. Tang, Y. Li, W. Yuan, B. Li, L. Tian, F. Liu, R. Hu, H. Gao, H. Wei, H. Zhang, H. Sun and B. Yang, *Chem. Commun.*, 2011, **47**, 6858–6860; (*f*) J. Shen, Y. Zhu, X. Yang and C. Li, *Chem. Commun.*, 2012, **48**, 3686–3699; (*g*) S. Zhu, Q. Meng, L. Wang, J. Zhang, Y. Song, H. Jin, K. Zhang, H. Sun, H. Wang and B. Yang, *Angew. Chem., Int. Ed.*, 2013, **52**, 3953–3957.

22 (*a*) K. Tak, R. Sharma, V. Dave, S. Jain and S. Sharma, *ACS Chem. Neurosci.*, 2020, **11**, 3741–3748; (*b*) A. Kumar, A. Kumari, P. Mukherjee, T. Saikia, K. Pal and S. K. Sahu, *Microchem. J.*, 2020, **159**, 105590.

23 R. S. A. Sonthanasamy, W. Y. W. Ahmad, S. Fazry, N. I. Hassan and A. M. Lazim, *Carbohydr. Polym.*, 2016, **137**, 488–496.

24 (*a*) E. Garcia-Calvo, P. Cabezas-Sanchez and J. L. Luque-Garcia, *Chemosphere*, 2021, **263**, 128170; (*b*) K. A. Horzmann and J. L. Freeman, *Toxicol. Sci.*, 2018, **163**, 5–12; (*c*) Y.-J. Dai, Y.-F. Jia, N. Chen, W.-P. Bian, Q.-K. Li, Y.-B. Ma, Y.-L. Chen and D.-S. Pei, *Environ. Toxicol. Chem.*, 2014, **33**, 11–17; (*d*) S. Cassar, I. Adatto, J. L. Freeman, J. T. Gamse, I. Iturria, C. Lawrence, A. Muriana, R. T. Peterson, S. Van Cruchten and L. I. Zon, *Chem. Res. Toxicol.*, 2020, **33**, 95–118.

25 G. S. Schorr, E. A. Falcone, D. J. Moretti and R. D. Andrews, *PLoS One*, 2014, **9**, e92633.

26 (*a*) D. Li, D. Wang, X. Zhao, W. Xi, A. Zebibula, N. Alifu, J.-F. Chen and J. Qian, *Mater. Chem. Front.*, 2018, **2**, 1343–1350; (*b*) Z. Peng, E. H. Miyanji, Y. Zhou, J. Pardo, S. D. Hettiarachchi, S. Li, P. L. Blackwelder, I. Skromne and R. M. Leblanc, *Nanoscale*, 2017, **16**, 17533–17543; (*c*) W. Liu, G. Huang, X. Su, S. Li, Q. Wang, Y. Zhao, Y. Liu, J. Luo, Y. Li, C. Li, D. Yuan, H. Hong, X. Chen and T. Chen, *ACS Appl. Mater. Interfaces*, 2020, **12**, 49012–49020.

27 (*a*) T. Deb, D. Choudhury, P. S. Guin, M. B. Saha, G. Chakrabarti and S. Das, *Chem. Biol. Interact.*, 2011, **189**, 206–214; (*b*) L. Isaacs, *Acc. Chem. Res.*, 2014, **47**, 2052–2062; (*c*) F. Zhang, Y.-H. Li, J.-Y. Li, Z.-R. Tang and Y.-J. Xu, *Environ. Pollut.*, 2019, **253**, 365–376.